ACS APPLIED MATERIALS & INTERFACES

Research Article

www.acsami.org

Electrocatalytic Hydrogen Evolution Reaction on Edges of a Few Layer Molybdenum Disulfide Nanodots

John Benson,[†] Meixian Li,[‡] Shuangbao Wang,[§] Peng Wang,[§] and Pagona Papakonstantinou*[,†]

[†]School of Engineering, Engineering Research Institute, Ulster University, Newtownabbey BT37 0QB, United Kingdom

[‡]College of Chemistry and Molecular Engineering, Peking University, Beijing 100871, People's Republic of China

[§]National Laboratory of Solid State Microstructures, College of Engineering and Applied Sciences and Collaborative Innovation Center of Advanced Microstructures, Nanjing University, 22 Hankou Road, Gulou, Nanjing 210093, People's Republic of China

Supporting Information

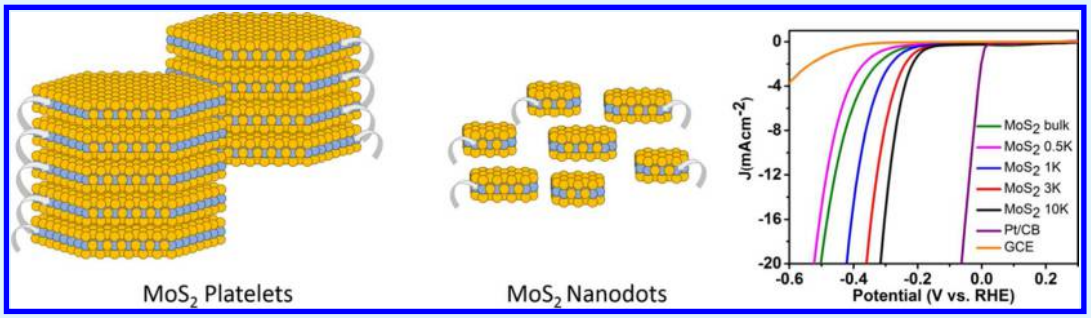

ABSTRACT: The design and development of inexpensive highly efficient electrocatalysts for hydrogen production underpins several emerging clean-energy technologies. In this work, for the first time, molybdenum disulfide (MoS_2) nanodots have been synthesized by ionic liquid assisted grinding exfoliation of bulk platelets and isolated by sequential centrifugation. The nanodots have a thickness of up to 7 layers (~4 nm) and an average lateral size smaller than 20 nm. Detailed structural characterization established that the nanodots retained the crystalline quality and low oxidation states of the bulk material. The small lateral size and reduced number of layers provided these nanodots with an easier path for the electron transport and plentiful active sites for the catalysis of hydrogen evolution reaction (HER) in acidic electrolyte. The MoS_2 nanodots exhibited good durability and a Tafel slope of 61 mV dec^{-1} with an estimated onset potential of −0.09 V vs RHE, which are considered among the best values achieved for 2H phase. It is envisaged that this work may provide a simplistic route to synthesize a wide range of 2D layered nanodots that have applications in water splitting and other energy related technologies.

KEYWORDS: *MoS_2 nanosheets, hydrogen evolution reaction, electrocatalysis, edges, nanodots, ionic liquid exfoliation, water splitting*

INTRODUCTION

Hydrogen is emerging as an ideal energy carrier for clean and sustainable energy technology.[1−4] Considerable effort has been directed toward the sustainable production of hydrogen from water splitting, which underpins several emerging clean-energy technologies. To be efficient, the process requires the presence of an electrocatalyst, to reduce the overpotential and drive the kinetically rate-limiting steps involved within reductive half reaction of water splitting, the hydrogen evolution reaction (HER: $2H^+ + 2e^- \rightarrow H_2$). Currently, expensive noble metal platinum is the most efficient electrocatalyst for improving the kinetics and efficiency of HER. Therefore, the discovery of active HER electrocatalysts made from earth-abundant elements constitutes a key step in the development of large-scale hydrogen production technology.[5−11]

Molybdenum disulfide (MoS_2) compounds have recently attracted considerable attention because of their appealing electrocatalytic properties for electrochemical as well as photochemical hydrogen evolution reaction (HER).[12−18] These favorable properties emanate from the presence of catalytically active sulfur atoms on the molybdenum edges of MoS_2 planes, a high stability in strong acids, and an advantageous band gap aligned with the hydrogen redox potential. MoS_2 has a layered packed structure consisting of a single layer of Mo atoms sandwiched between two layers of sulfur atoms in a trigonal prismatic arrangement. These stacks are piled in a graphite-like-manner to form bulk material, held together by weak van der Waals forces. Bulk MoS_2 is a semiconductor with an indirect bandgap of 1.3 eV, which is modified to a direct band gap semiconductor of 1.8 eV, when it is thinned down to a few layers. Theoretical studies have identified that the unsaturated S atoms located at the edges of MoS_2 can absorb H with a small free energy ($\Delta G_H^0 \approx 0.08$ eV)[19,20] and hence act as active sites for HER. This prediction was further confirmed experimentally on MoS_2 nanoparticles by systematically varying terrace and edge site densities, where a

Received: April 19, 2015
Accepted: June 8, 2015
Published: June 8, 2015

DOI: 10.1021/acsami.5b03399
ACS Appl. Mater. Interfaces 2015, 7, 14113−14122

linear correlation between the exchange current density and MoS_2 edge length was established.[20] As a result, efforts have been focused on exposing the catalytic edge sites by engineering the morphology of MoS_2.[21−25] In this context, various strategies have been explored through the development of various nanostructures in the form of ordered architectures, vertically aligned nanosheets, flowerlike nanosheets, microboxes, and nanoparticles.[26−29]

Although a plethora of active edge sites is beneficial, the vertical charge transport through the layers is an important limitation in HER performance. This needs to be addressed in the design of MoS_2 electrocatalysts with optimum performance. Theoretical studies have predicted and experimental studies have confirmed that the electronic structure of MoS_2 edges is dominated by metallic one-dimensional edge states,[30] which is in sharp contrast to the semiconducting basal plane. As a result, the electrocatalysis of atomically thin CVD grown MoS_2 films has been found to be strongly dependent on the layer number, which was correlated to the hopping of electrons in the vertical direction of MoS_2 layers. These observations led us to the proposition that MoS_2 nanodots, that is, a few layer MoS_2 sheets with very small lateral dimensions, should show enhanced catalytic activity due to a simultaneous increase in unsaturated sulfur edge sites and enhanced electron transfer accrued from the reduced number of layers. Therefore, it is intuitive to construct a scalable method to produce few layer MoS_2 nanodots to optimize the catalytic performance for HER. To date, the HER activity from MoS_2 nanodots is largely unexplored, which stems mainly from the lack of methods to produce these in appreciable amounts.

Today the synthesis of MoS_2 nanodots has been mainly connected with the investigation of photoluminescence arising from quantum confinement effects rather than assessment of HER activity.[31−34] So far top down synthesis of few-layered MoS_2 nanodots with lateral dimensions smaller than 50 nm is based either on exfoliation of bulk MoS_2 using ultrasonication in suitable organic solvents or on a combination of grinding and ultrasonication, or on electrochemical exfoliation.[24,25,31−34] Generally, the synthesis of MoS_2 nanodots is under intensive investigation, however evaluation of their quality and performance for various applications including energy storage, catalysis, gas sensing, and optoelectronic devices has been largely unexplored.

Here, we report the synthesis of MoS_2 nanodots using optimized experimental conditions, which involve grinding MoS_2 platelets in a small quantity of room temperature ionic liquid (RTIL) followed by sequential centrifugation steps. As schematically depicted in Figure 1, the combined compressive, torsional, and shear forces exerted on the MoS_2 platelets are able to exfoliate and at the same time break up the bulk crystals. During the grinding process, the RTIL acts as a lubricant, which allows low friction between the moving pestle and mortar, hence facilitating the exfoliation. RTILs are salts composed of large, asymmetric, and charge delocalized cations that are paired with anions having significantly different chemical structure and symmetry. This incompatibility of the chemical structures inhibits crystallization at room temperature and allows them to have a unique combination of characteristics, including thermal stability, nonflammability, and negligible volatility, which make them attractive as lubricants.[35]

We show that the HER activity of nanosized MoS_2 is substantially improved, when compared to thicker and larger nanoplatelets. We found that MoS_2 nanodots exhibit excellent electrocatalytic activity with low overpotential, mainly attributed to the large number of exposed active conductive edges of MoS_2 and to the low number of layers.

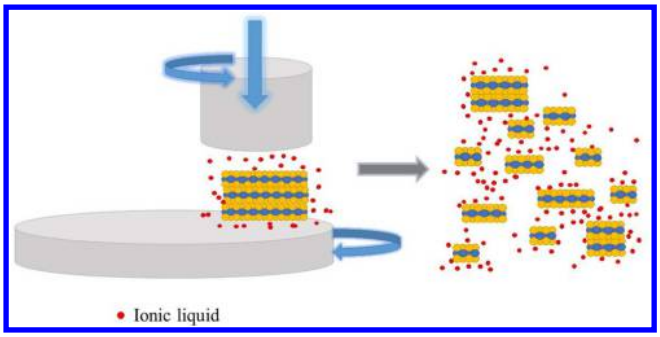

Figure 1. Schematic representation of the ionic liquid assisted grinding exfoliation process. Grinding of MoS_2 platelets in the presence of room temperature ionic liquid (RTIL) produces a gel structure, with the ionic liquid acting as a lubricant. Combined compressive, torsional, and shear forces exerted on MoS_2 platelets in the presence of a small amount of RTIL are able to exfoliate and at the same time break up the bulk crystals.

SYNTHESIS

The synthesis of MoS_2 nanodots was carried out in a planetary grinding machine using high purity MoS_2 powder with a sufficient amount of RTIL (1-butyl-3-methylimidazolium hexafluorophosphate, $BMIMPF_6$) to produce a gelatinous material.[36−39] During grinding, the RTIL protects every newly exposed MoS_2 surface by adsorbing onto the surface, keeping the sheets separated and avoiding restacking. The adsorption of ionic liquids onto the MoS_2 surface is believed to be dominated by weak noncovalent interactions.[40]

The resulting gel was subjected to three washing steps in a mixture of DMF (*N*,*N*-dimethylformamide) and acetone to remove the RTIL.[36] The formation of MoS_2 nanodots is purely a mechanical effect, which arises mainly from the compressive forces exerted during the grinding process. The yield of the nanodots increases by prolonging the duration of grinding. It is worth noting that the mechanical breaking point of MoS_2 is 5 times smaller than that of graphene,[41] leading to the overall smaller lateral size.

The clean ground product consisted of an assortment of sheets of various sizes and thicknesses, which were size selected by sequential centrifugation as schematically illustrated in Figure 2. Briefly the dispersion of the washed ground product was initially centrifuged at 500 rpm, which resulted in a pellet comprised of large unexfoliated flakes. The supernatant from 500 rpm run was then centrifuged at 1000 rpm to isolate sheets with smaller thickness and lateral dimensions. The procedure was repeated using centrifugations at 3000 and 10 000 rpm, as described earlier.[37] Isolated products are labeled MoS_2 *X*K, where *X*K represents the centrifugation speed in thousands of rpm.

RESULTS AND DISCUSSION

SEM images of MoS_2 bulk together with those of isolated MoS_2 fractions separated at different sequential centrifugation steps are displayed in Figure 3. MoS_2 bulk consists predominantly of large platelets (~20 μm), as well as a wide range of smaller flake sizes stacked on larger platelets as shown in Figure 3a. Grinding in ionic liquid breaks and exfoliates MoS_2 producing a collection of nanosheets of various sizes and thicknesses. Size

DOI: 10.1021/acsami.5b03399
ACS Appl. Mater. Interfaces 2015, 7, 14113−14122

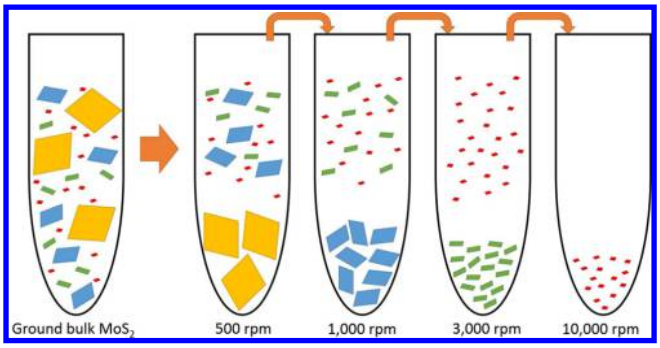

Figure 2. Schematic representation of the sequential centrifugation process. Sequential centrifugation of the supernatant at progressively higher speeds allows the isolation of thinner and smaller particles. Large and thick platelets produce a pellet using low centrifugation speeds and small durations. Thinner and smaller sheets are pelleted at higher speeds and longer durations.

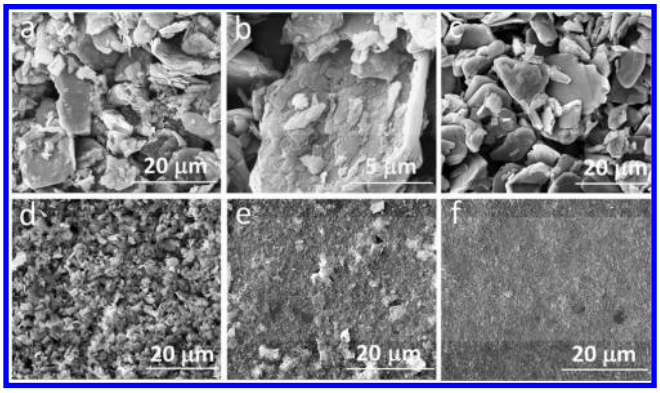

Figure 3. SEM images of isolated sediment: (a) MoS_2-bulk, (b) zoomed area of MoS_2 bulk, (c) MoS_2 0.5K, (d) MoS_2 1K, (e) MoS_2 3K, and (f) MoS_2 10K.

selection was achieved by subjecting the DMF dispersion of ground washed MoS_2 to progressive centrifugation steps, by removing the sediment and subjecting the supernatant to increasing centrifugation speeds. Separation is based on size and density, with larger and thicker (heavier) platelets withdrawing at lower centrifugation speeds (forces), while smaller and lighter particles withdraw at higher speeds. This is evidenced clearly in Figure 3c, where centrifugation at the low speed of 500 rpm withdrew predominantly the large and thick platelets (Figure 3c) leaving in the supernatant an assortment of smaller and lighter material. Subsequent centrifugation of the supernatant at 1000 rpm withdrew ground fragments around 1−6 μm in lateral size, whereas higher centrifugation speeds separated finer material successfully (smaller and thinner) as schematically illustrated in Figure 2. The majority of MoS_2 3K isolated sediment has lateral sizes smaller than 70 nm with a small contribution from larger flakes of about 1−4 μm in lateral size as confirmed by atomic force microscopy (AFM, Figure 4e and g). MoS_2 10K isolated sediment is populated with nanodots smaller than 20 nm in size and up to 7 layers in thickness (Figure 4a and Supporting Information Figure S1). The highly parallel and ordered lattice planes in high-resolution TEM (HRTEM) images of MoS_2 10K (Figure 4a) are clearly visible. The *d*-spacing of 0.3125 nm, which corresponds to the (004) faces of MoS_2 crystals, indicates that the nanodots retained their crystalline quality after the ionic liquid assisted grinding exfoliation. The clean exfoliated MoS_2 nanosheets have a proneness to restack due to the van der Waals interactions (Figure 4b),[33] which gives rise to multiple sets of rotated spots of variable intensity in the SAED pattern (Figure 4c) and ring motifs. In addition, MoS_2 nanodots show a distinct tendency to form agglomerates most probably due to a predisposition to minimize their surface energy by stabilization of the dangling bonds at the edges of the crystals.[40] Overall, the results show that the grinding process allows the high crystalline quality to remain intact in the resulting nanodots. This result is different from our previous work, which reported the presence of amorphous ultrasmall MoS_2 nanoparticles using ultrasonication in DMF and centrifugation steps.[25]

The optical properties of MoS_2 centrifugation products dispersed in DMF were investigated by UV−vis absorption spectroscopy and are shown in Figure 5a. The MoS_2 10K dispersion exhibited four optical absorption peaks at 413.1, 465.5, 617.1, and 677.9 nm, which are characteristic fingerprints of well exfoliated MoS_2 nanosheets of 2H type with trigonal prismatic coordination.[42,43] The two well-defined peaks

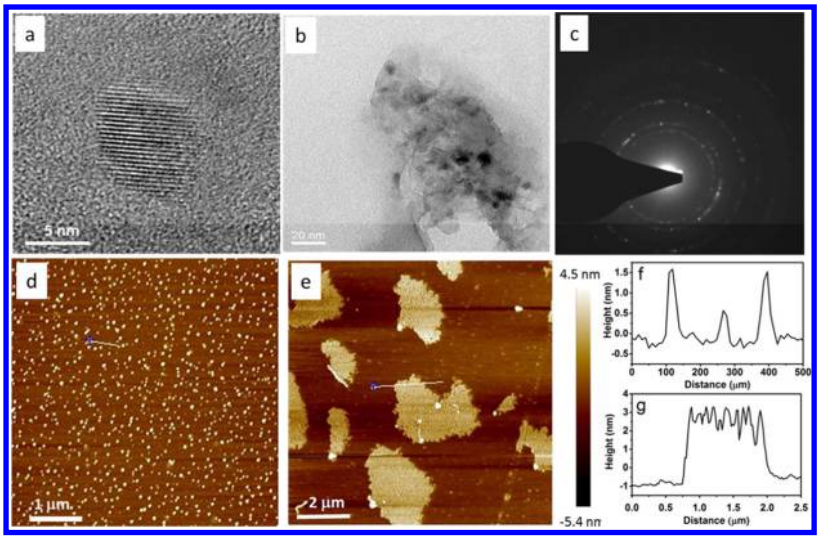

Figure 4. High-resolution TEM images of (a) MoS_2 10K nanodot, (b) agglomeration of nanodots, and (c) SAED pattern of (b). AFM image of (d) MoS_2 10K and (e) MoS_2 3K with corresponding height profiles shown in (f) and (g), respectively.

DOI: 10.1021/acsami.5b03399
ACS Appl. Mater. Interfaces 2015, 7, 14113−14122

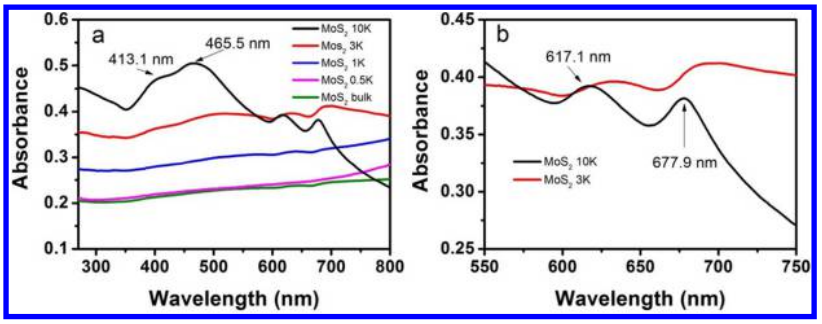

Figure 5. (a) UV−vis absorption spectrum for all MoS_2 products dispersed in DMF. (b) Noticeable blue shift for the MoS_2 10K relative to MoS_2 3K, due to a reduction in thickness and lateral dimensions.

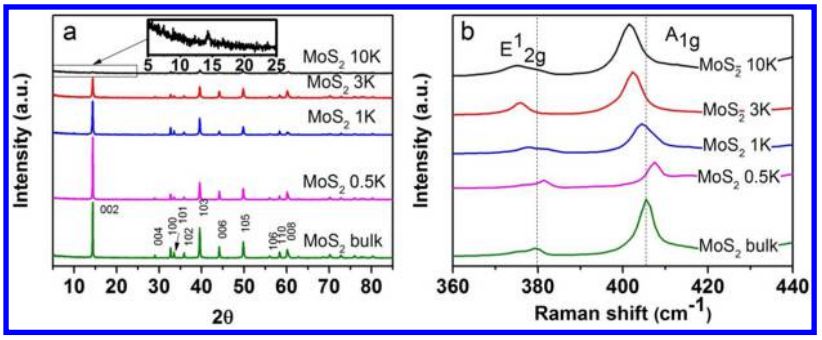

Figure 6. (a) XRD diffraction patterns of MoS_2-bulk and isolated sediments. Reduction in (002) peak intensity is associated with progressive exfoliation. (b) Raman spectra were measured using 632.8 nm laser. Significant red shift of A_{1g} mode for increased centrifugation speeds indicates reduction in the number of layers.

centered at 617.1 and 677.9 nm are due to the direct excitonic transitions at the K point of the Brillouin zone.[44,45] The broader peaks at 413.1 and 465.5 nm are assigned to the direct transition from the deep valence band to the conduction band.[46] However, for lower centrifugation speeds, the Mie scattering induced background was substantially reduced and the spectra appeared flatten with less distinct peaks, indicating a transition from direct to indirect bandgap, a characteristic of thicker flakes. In addition, MoS_2 10K absorption spectra displayed a blue-shift versus the rest of the products (Figure 5b), which is consistent with quantum confinement effects arising from thickness and lateral size reduction.[32]

X-ray diffraction (XRD) patterns were used to determine the evolution of structural changes at various stages of the sequential centrifugation process (Figure 6a). MoS_2 bulk exhibits a distinctive intense (002) peak, centered at 14.4°, corresponding to an interlayer *d*-spacing of 0.614 nm. In addition, various weak diffraction reflections from the (100), (103), (006), (105), and (008) planes were observed at higher angles, characteristic of polycrystalline MoS_2. No substantial change in the (002) peak was observed for MoS_2 0.5K due to the exposure of large and highly crystalline platelets as revealed by SEM images of Figure 3c. However, higher centrifugation speeds caused a progressive decrease in (002) peak intensity, with MoS_2 10K sediment retaining only 3.4% of the bulk intensity. A similar decrease in the diffraction intensity of the (002) graphite peak was observed in the sequential centrifugation products from ground graphite.[37] Because the diffraction peak intensity is a result of constructive interference from aligned crystal planes, a decrease in the diffraction intensity indicates a reduction in the number of aligned planes (layers), with zero intensity expected from completely exfoliated MoS_2.[47,48] The presence of a weak (002) signal from the MoS_2 10K indicates that the nanodots consist of a few layers, which is in agreement with the AFM results (Figure 4d). In addition, a progressive increase in fwhm was observed for centrifugation speeds equal to or higher than 1000 rpm (Supporting Information Table S1), further confirming the decrease in lateral size.

Raman spectroscopy was used to assess the exfoliation of the products employing a He−Ne laser (632.8 nm excitation wavelength) with a beam size of approximately 2 μm. Figure 6b shows characteristic Raman peaks associated with E_{2g} (in-plane motion of Mo and S in opposite directions) and A_{1g} (out-of-plane motions of S atoms) active modes located at 379.5 and 405.4 cm^{-1}, respectively.[49−51] It is well established that the addition of extra layers on MoS_2 leads to the stiffening of the out-of-plane phonon modes, resulting in a downward-shift of the A1g mode. Here, the A_{1g} mode is up-shifted by approximately 2.1 cm^{-1} from bulk to MoS_2 0.5K (405.4 to 407.5 cm^{-1}), which indicates that the MoS_2 0.5K platelets are thicker than the bulk ones.[51] Although at first sight this result seems rather counter-intuitive, it can be explained bearing in mind the SEM and XRD results (Figures 3a,c and 6a), which show that centrifugation at 500 rpm was very efficient in isolating large and thick platelets, free from small size debris. In contrast, the bulk material besides the large and thick platelets is populated with smaller and finer flakes (Figure 2b), which give rise to the upshift of 2.1 cm^{-1}. Centrifugation at speeds higher than 1000 rpm gave rise to a noticeable downshift (404.4 cm^{-1}) in the A_{1g} mode, indicating a reduction in thickness, as flakes were exfoliated to a few layers. This A_{1g} energy upshift suggests that the electron density in exfoliated MoS_2 is enhanced most probably due to an increased number of edges, which are electron rich.[52] The peak position of E_{2g} mode shifts to smaller wavenumbers, and both Raman modes

DOI: 10.1021/acsami.5b03399
ACS Appl. Mater. Interfaces 2015, 7, 14113−14122

are narrowed with increasing centrifugation speeds. These variations are in agreement with previous Raman studies on MoS_2 quantum dot/nanosheets hybrids[31] and are related to an increase in disorder associated with edge defects because the average nanosheet later size is smaller than the laser spot diameter.

The elemental composition of the five catalysts was characterized using X-ray photoelectron spectroscopy (XPS). The wide survey scan of bulk and MoS_2 10K can be seen in Figure S2a (Supporting Information). The clear presence of C and O elements for all catalysts is associated with adventitious impurities, which originate from the solvent[53] and the atmosphere. Stoichiometric ratios of S to Mo calculated from the respective integrated areas are close to 2:1 (1.95 ± 0.05:1), demonstrating the expected MoS_2 phase. As shown in Figure 7a,b, all of the sediments exhibited almost the same binding

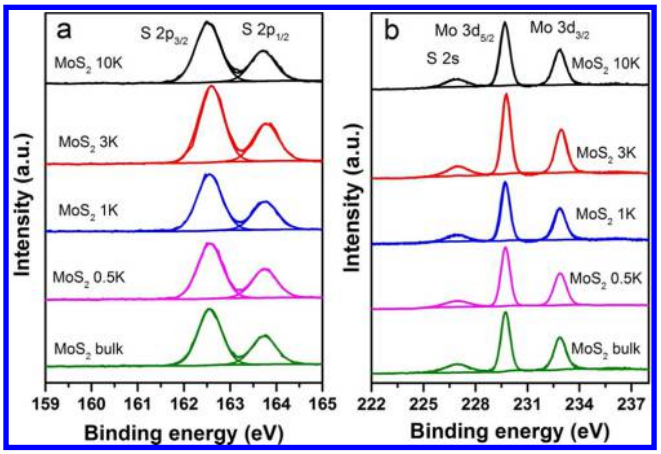

Figure 7. High-resolution (a) S 2p and (b) Mo 3d XPS spectra of the five catalysts. S and Mo contents were calculated to have a ratio of 2:1, corresponding to MoS_2 phase.

energies for well-defined S and Mo doublets as those of MoS_2 crystal. The peaks around 162.0 and 163.2 eV correspond to S $2p_{3/2}$ and S $2p_{1/2}$ orbitals, respectively (Figure 7a), while the peaks at 229.2 and 232.4 eV are attributed to Mo $3d_{5/2}$ and Mo $3d_{3/2}$ orbitals, respectively. These peak positions are indicative of Mo^{4+} and S^{2-} oxidation states in 2H phase of MoS_2.[12,25] Binding energies of S 2p and Mo 3d regions remained constant before and after grinding, indicative of no changes in the oxidation states.

The fwhm of Mo $3d_{5/2}$ peak increased from 0.60 to 0.67 for MoS_2 bulk and MoS_2 10K respectively. Similarly, the fwhm of S $2p_{3/2}$ was increased from 0.59 for bulk to 0.67 at a centrifugation speed of 10K rpm. The atomic concentration of O 1s increased only by 2.31 at. % from bulk (9.60 + 0.59 at. %) to MoS_2 10K (11.91 + 0.84 at. %) (Supporting Information Figure S2b and Table S2). These data indicate only a minute transformation of sulfide to oxide and Mo to Mo−O with progressive isolation of smaller and thinner flakes. Furthermore, no noticeable peaks from either Mo higher oxidation states (Mo^{5+} or Mo^{6+}) at higher energies of ∼236 eV, nor from S higher oxidation states, in the energy region 168−170 eV, were observed,[25] confirming that there is no obvious oxidation of MoS_2 nanodots. This is different from the majority of studies on MoS_2 nanodots or nanosized flakes, where a significant change in the oxidation state occurs upon exfoliation.[33,53,54] The possible reason is that the ionic liquid protects the sheets and inhibits oxidation of MoS_2 during exfoliation. This is similar to our previous work,[30] where we reported the production of low oxygen content, few layer graphene nanosheets by RTIL assisted grinding exfoliation. The presence of predominant low oxidation states of Mo might play a role in the electron filling of bonding and antibonding between the active sites and H, lowering the H bonding energy and activation barrier and thus improving the HER activity.

The HER activities of the five MoS_2 catalysts were investigated in 0.5 M H_2SO_4 in a three-electrode setup, using a GCE electrode (3 mm diameter) with a mass loading of 0.28 mg/cm^2. Comparison of polarization curves is provided in Figure 8a together with those of glassy carbon electrode and Pt/C catalyst (20 wt % Pt). An *iR* correction has been employed to compensate for any potential loss arising from external resistance of the electrochemical system in this figure as explained in the Supporting Information (electrochemical measurements). It can be clearly seen that the catalytic activities of H_2 generation increased with the decrease in lateral size and number of layers, upon sequential centrifugation. The MoS_2 10K, in particular, shows the best catalytic performance exhibiting an onset potential of −0.09 V vs RHE and an overpotential (η_{10}) of −248 mV at the cathodic current density of 10 mA/cm^2; the last is commonly used as a figure of merit for comparing the HER performance of electrocatalysts.[14,55] Both potentials are considerably more positive than those of MoS_2 bulk, displaying an onset potential of −0.18 V and η_{10} = −471 mV. MoS_2 0.5K shows inferior characteristics as compared to the bulk due to the absence of fine and small flakes in agreement with the SEM, XRD, and Raman results.

It is well understood that the electronic structure of catalysts can affect HER catalytic activity, as it will affect the Gibbs free energy for hydrogen adsorption on the catalyst and the electron transfer between the catalysts, the reagents, and the electrode.

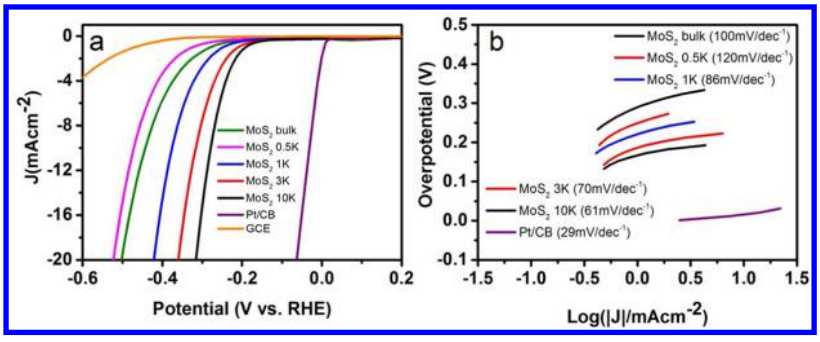

Figure 8. (a) Polarization curves of all five catalysts. GCE and Pt/CB (20 wt % Pt) are used as comparison. (b) Tafel slopes of all five catalysts.

DOI: 10.1021/acsami.5b03399
ACS Appl. Mater. Interfaces 2015, 7, 14113−14122

By reducing the dimensions along both the in-plane and the vertical directions, a considerable number of metallic edges becomes available for hydrogen adsorption, and at the same time an easier path for transport of electrons is availed, all of which contribute to the improved catalytic activity for HER. The increase in the number of active sites for MoS_2 10K nanodots as compared to other catalysts was confirmed by the observed larger double layer capacitance (C_{dl}), that is, the effective electrochemically active surface area.[56] Cyclic voltammograms (CVs) were collected in the region of 0.33−0.13 V, where the current response should only be due to the charging of the double layer (Supporting Information Figures S3 and S4). The capacitance of MoS_2 10K is 3.5 times larger than that of MoS_2 bulk.

Tafel slope is a useful metric to assess the performance of catalysts and at the same time is a valuable indicator of the mechanistic reaction processes of HER.[57−59] The linear portions of Tafel plots were fitted to the Tafel equation ($\eta = b \log|J| + a$, where η is overpotential, J is the current density, a is exchange current density, and b is the Tafel slope) and yielded the Tafel slope (Figure 8b). A small Tafel slope is preferred as it indicates a fast increase of hydrogen generation rate with the applied overpotential. Tafel slopes for all catalysts are summarized in Supporting Information Table S3 and are plotted in Figure 8b, which clearly show a trend from high to low slope as the lateral size and thickness decrease. The Tafel slope of 61 mV dec^{-1} for MoS_2 10K is superior to several published works, listed in Table 1, such as MoS_2 nanodots prepared by sonication (Ji et al.,[60] onset = −0.12 V, Tafel = ∼70 mV dec^{-1}), mechanical (Varrla et al.,[61] Tafel = 115 mV dec^{-1}), or electrochemical methods (Gopalakrishnan et al.,[34] onset = ∼ −0.21 V (vs SHE), Tafel = 60 mV dec^{-1}). To the best of our knowledge, MoS_2 nanodots synthesized here are the most efficient MoS_2 with 2H phase. The low oxidation state of the MoS_2 10K nanodots achieved by our synthesis process is one important factor contributing to their superior performance. It is well established that edge oxidized 2H phase nanosheets show a dramatically suppressed performance (slope 186 mV dec^{-1}) caused by the deactivation of edges.[33,53,54]

Table 1. Comparison of HER Activity of MoS_2 10K with Other Relevant Reported Findings

HER catalyst	onset potential (V)	Tafel slope (mV dec^{-1})	ref
MoS_2 10K	−0.09 (0.19 at 1 mA cm^{-2})	61	this work
MoS_2 composite (NMP)	−0.12	69	33
MoS_2 nanosheets	−0.27 (at 1 mA cm^{-2})	115	61
MoS_2 dots on Au	−0.16	82	24
MoS_2 embedded in ordered mesoporous carbon	(∼)−0.12	60−65	62
MoS_2 dots/nanosheet hybrid on Au	−0.19	74	31
MoS_2 nanoparticles on Au	−0.09	69	25
Li−MoS_2		62	63
MoS_2 composite (NMP)	−0.12	69	33
MoS_2 nanoplate assemblies	−0.09	68	48
NSs-550		68	64
$V_{0.09}Mo_{0.91}S_2$ (vanadium doped MoS_2)	−0.13	69	65

According to the classic theory, hydrogen evolution proceeds through three principal reaction steps in acidic media:[57,66]

$$H_3O^+ + e^- \rightarrow H_{ad} + H_2O \quad \text{Volmer reaction (Tafel slope 120 mV } dec^{-1}) \quad (1)$$

$$H_{ad} + H_3O^+ + e^- \rightarrow H_2 + H_2O \quad \text{Heyrovsky reaction (Tafel slope 40 mV } dec^{-1}) \quad (2)$$

$$2H_{ad} \rightarrow H_2 \quad \text{Tafel reaction (Tafel slope 30 mV } dec^{-1}) \quad (3)$$

where H_{ad} represents the hydrogen adsorption sites onto the surface of a metal catalyst. According to theory, the slopes associated with Volmer, Heyrovsky, and Tafel reactions are 120 mV dec^{-1} (eq 1), 40 mV dec^{-1} (eq 2), and 30 mV dec^{-1} (eq 3), respectively. Experimentally two main pathways are generally observed for HER, Volmer−Heyrovsky reaction (eqs 1 and 2), and Volmer−Tafel reaction (eqs 1 and 3).[67,68] In the present study, the Tafel slope of 61 mV dec^{-1} for MoS_2 10K suggests that HER was most probably controlled by both electron reduction of protons, which provides a hydrogen atom bound to an active site (eq 1), and electrochemical desorption of hydrogen (eq 2) (Volmer−Heyrovsky reaction). In contrast, for crystalline MoS_2 bulk, the HER proceeds through the Volmer reaction, as suggested by its large Tafel slope of 100 mV dec^{-1}. For both MoS_2 bulk and MoS_2 0.5K (120 mV dec^{-1}), the reaction kinetics are limited by the inefficient number of edges, where adsorption of H^+ takes place, as indicated by the large Tafel slope.[14] At higher centrifugation speeds, the lower Tafel slopes suggest that the number of accessible active sites on the 2H phase MoS_2 nanosheets has increased.

The intrinsic activity of the catalyst materials was studied using the turnover frequency (TOF), which represents the number of hydrogen molecules produced per second per active site.[23,69]

TOF of MoS_2 10K at −0.2 V (3.3 H_2/s per active site) was more than 4 times higher than that of MoS_2 bulk (0.7 H_2/s per active site), highlighting the important influence of exfoliation and small lateral size in HER activity (Figure 9). The TOF value obtained for MoS_2 10K shows a turnover frequency (TOF) of 3.3 H_2/s at an overpotential of −0.2 V, thus outperforming MoO_3−MoS_2 nanowires[70] (∼0.7 H_2/s at −0.2 V) and double gyroid MoS_2[23] (∼0.7 H_2/s at −0.2 V) as shown in Supporting Information Table S4. These results reveal that the combination of decreased particle size, thickness, and high

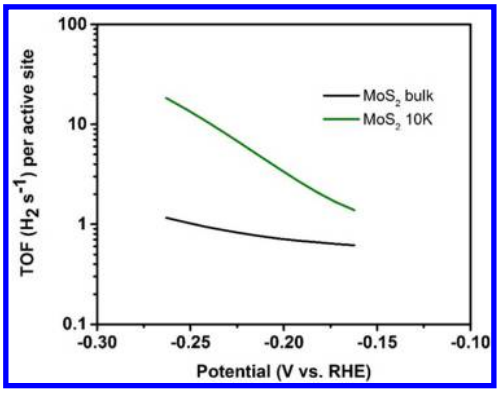

Figure 9. Turnover frequencies of MoS_2 10K and MoS_2 bulk. TOF calculations were conducted per Mo atom.

DOI: 10.1021/acsami.5b03399
ACS Appl. Mater. Interfaces 2015, 7, 14113−14122

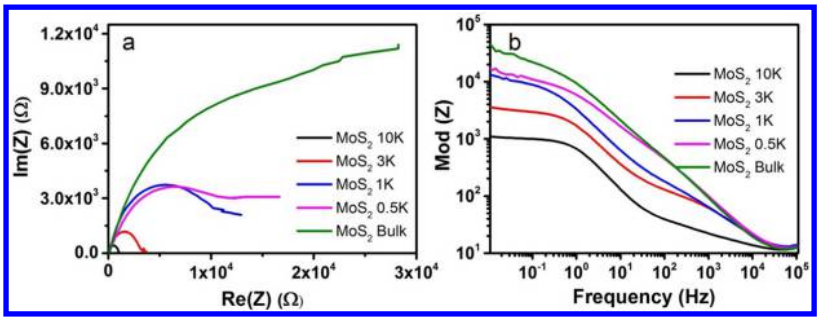

Figure 10. EIS plots in the form of (a) Nyquist and (b) Bode plots of the five catalysts. Measurements were performed at −0.22 V vs RHE.

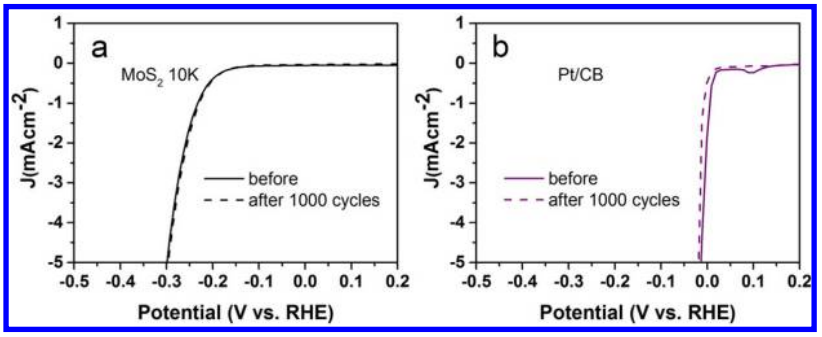

Figure 11. Polarization curves of (a) MoS_2 10K and (b) commercial Pt/CB (20 wt % Pt) before and after 1000 CV scans. All measurements were carried out in 0.5 M H_2SO_4 using a 3 mm diameter BASI GCE and a catalyst loading of 0.283 mg/cm^2.

crystallinity is highly beneficial for the greatly enhanced electrocatalytic activity and the stability of MoS_2.

One should note that a critical issue in calculating accurately TOF originates from the precision in measuring the number of active sites (n) and the electrochemically active surface area (ECSA). The above TOF calculations were conducted assuming that the surface exposed Mo atoms are the active sites. However, for crystalline 2H-MoS_2, only exposed edge sites contribute to HER activity. Such an uncertainty would lead to inaccuracies in the magnitude of the actual TOF.

The estimation of electrochemically active surface area was conducted by measurement of the double-layer capacitance in a potential region with no faradaic response following McCory et al.'s methodology.[71] The ESCA was estimated from the ratio of the measured double layer capacitance with respect to the specific capacitance of an atomically smooth MoS_2 material (~60 μF/cm^2).

$$\mathrm{ECSA} = \frac{C_{\mathrm{dl}}\ (\mathrm{mF\ cm^{-2}})}{C_{\mathrm{dl}}\ (\mu\mathrm{F\ cm^{-2}})} \quad (4)$$

Using eq 4, we have obtained values of 35.83 and 10.32 for the ESCA of MoS_2 10K and MoS_2 bulk, respectively (Supporting Information Table S3). However, this method, although suitable for electrodes consisting of conductive materials, could lead to error in the ECSA determination for semiconducting layers, such as 2H-MoS_2, where an increase in active surface area does not necessarily translate into an increase in the double layer capacitance. These uncertainties in the estimation of both n and ESCA in Supporting Information eq S2 can lead to estimated TOFs that differ by orders of magnitude. These factors make it difficult to conduct meaningful comparisons of TOFs with the literature. In addition, for different MoS_x-based catalysts, the comparison of the TOFs is only meaningful when the value is taken at the same overpotential.

The electrode kinetics under catalytic HER operating conditions (Figure 10) were investigated by electrochemical impedance spectroscopy (EIS). The impedance spectra mirror the HER activity, by applying a small voltage (−0.22 V) close to the onset potential. A high HER activity is reflected by a small semicircle in the Nyquist plot ($Re(z)$ vs $Im(z)$ over the frequency range from 1 MHz to 10 mHz), which indicates a small charge transfer resistance (R_{ct}) as it allows fast shuttling of electrons during HER (Figure 10a). This is obvious in the Bode plot, which presents the modulus of impedance $|Z| = (|Re(Z)|^2 + |Im(Z)|^2)^{1/2}$ as a function of log of frequency (Figure 10b). In the low frequency regime, it is obvious that the modulus of Z is the smallest for MoS_2 10K nanodots. It is clear that as exfoliation products are reduced both in lateral size and in thickness, the R_{ct} dramatically decreases. This trend is consistent with those of Tafel slopes and polarization curves. These electrochemical data, together with the structural characterization results, consistently show a dramatic increase in intrinsic electrocatalytic activity for HER as the products evolve from large and thick platelets to a few layer nanodots.

The activity of both MoS_2 10K and commercial Pt/CB (20 wt % Pt) before and after application of 1000 cycles (between +0.2 and −0.4 V vs RHE at a scan rate of 100 mVs^{-1}) is presented in Figure 11a,b. No measurable change was observed for MoS_2 10K. In contrast, the Pt/CB exhibited a noticeable shift after 1000 cycles. The results reveal the exceptional stability of MoS_2 10K, which are in agreement with the well reported stability of crystalline 2H-MoS_2. This is linked to the ability of crystalline MoS_2 to resist oxidation in contrast to amorphous MoS_2, which is more susceptible to oxidation.[72] However, it should be noted that intense stability tests in excess of 10 000 potential cycles are required for real working devices.

DOI: 10.1021/acsami.5b03399
ACS Appl. Mater. Interfaces 2015, 7, 14113−14122

CONCLUSIONS

In summary, we demonstrate the exfoliation of MoS_2 sheets via a simple ionic liquid assisted grinding method combined with sequential centrifugation steps. MoS_2 nanodots having a thickness of up to 7 layers (~4 nm) and an average lateral size smaller than 20 nm were isolated through sequential centrifugation steps. A drastic increase in catalytic H_2 evolution was observed with a simultaneous decrease in number of layers and lateral size. The obtained MoS_2 nanodots exhibit an onset potential as small as −0.09 mV, a high exchange current density of 1.6×10^{-3} mA cm^{-2}, and a Tafel slope of 61 mV dec^{-1}. Moreover, they merely require overpotentials as low as −248 mV to attain current densities of 10 mA cm^{-2} and show good long-term stability. All these characteristics compare favorably to all recently reported MoS_2 quantum dots or nanosheet catalysts having 2H phase. The improved catalytic activity can be attributed to the following factors: (i) the high abundance of edge sites exposing S edge atoms, which play a crucial role in catalyzing the electrochemical HER, (ii) the high degree of exfoliation (reduced number of layers,) which allows efficient electron transfer between the electron rich edges and the electrode, and (iii) the low oxidation state of the 2H-MoS_2 nanodots, which substantially improves the charge transfer kinetics of HER. We have demonstrated that the HER performance of MoS_2 varies significantly with size and thickness reduction and hence provides fundamental insight for future theoretical and experimental research. The novel fabrication method reported here is scalable and can be extended to obtain other 2D layered-based catalysts and therefore represents an important development toward water splitting and other energy conversion technologies.

ASSOCIATED CONTENT

Supporting Information

Experimental details, AFM of MoS_2 10K, XPS wide spectra, core level O 1s spectra, double layer capacitance measurements, XRD, and electrochemical data. The Supporting Information is available free of charge on the ACS Publications website at DOI: 10.1021/acsami.5b03399.

AUTHOR INFORMATION

Corresponding Author

*E-mail: p.papakonstantinou@ulster.ac.uk.

Notes

The authors declare no competing financial interest.

ACKNOWLEDGMENTS

This work was financially supported by a Ph.D. Studentship to J.B. from the Department of Employment and Learning in Northern Ireland; a visiting Senior Research Fellowship to M.L. by Ulster University; and the Chinese thousand-talents plan program and the Jiangsu Shuangchuang program (P.W.).

REFERENCES

(1) Walter, M. G.; Warren, E. L.; McKone, J. R.; Boettcher, S. W.; Mi, Q.; Santori, E. A.; Lewis, N. S. Solar Water Splitting Cells. *Chem. Rev.* **2010**, *110*, 6446−6473.

(2) Lewis, N. S. Toward Cost-Effective Solar Energy Use. *Science* **2007**, *315*, 798−801.

(3) Nocera, D. G. The Artificial Leaf. *Acc. Chem. Res.* **2012**, *45*, 767−776.

(4) Lewis, N. S.; Nocera, D. G. Powering the Planet: Chemical Challenges in Solar Energy Utilization. *Proc. Natl. Acad. Sci. U.S.A.* **2006**, *103*, 15729−15735.

(5) Morales-Guio, C. G.; Hu, X. Amorphous Molybdenum Sulfides As Hydrogen Evolution Catalysts. *Acc. Chem. Res.* **2014**, *47*, 2671−2681.

(6) Wang, M.; Chen, L.; Sun, L. Recent Progress in Electrochemical Hydrogen Production with Earth-Abundant Metal Complexes As Catalysts. *Energy Environ. Sci.* **2012**, *5*, 6763−6778.

(7) Yan, Y.; Xia, B.; Xu, Z.; Wang, X. Recent Development of Molybdenum Sulfides as Advanced Electrocatalysts for Hydrogen Evolution Reaction. *ACS Catal.* **2014**, *4*, 1693−1705.

(8) Morales-Guio, C. G.; Stern, L. A.; Hu, X. Nanostructured Hydrotreating Catalysts for Electrochemical Hydrogen Evolution. *Chem. Soc. Rev.* **2014**, *43*, 6555−6569.

(9) Faber, M. S.; Jin, S. Earth-Abundant Inorganic Electrocatalysts and Their Nanostructures for Energy Conversion Applications. *Energy Environ. Sci.* **2014**, *7*, 3519−3542.

(10) Laursen, A. B.; Kegnæs, S.; Dahl, S.; Chorkendorff, I. Molybdenum Sulfides−Efficient and Viable Materials for Electro- and Photoelectrocatalytic Hydrogen Evolution. *Energy Environ. Sci.* **2012**, *5*, 5577.

(11) Thoi, V. S.; Sun, Y.; Long, J. R.; Chang, C. J. Complexes of Earth-Abundant Metals for Catalytic Electrochemical Hydrogen Generation under Aqueous Conditions. *Chem. Soc. Rev.* **2013**, *42*, 2388−2400.

(12) Vrubel, H.; Merki, D.; Hu, X. Hydrogen Evolution Catalyzed by MoS_3 and MoS_2 Particles. *Energy Environ. Sci.* **2012**, *5*, 6136.

(13) Vesborg, P. C. K.; Seger, B.; Chorkendorff, I. Recent Development in Hydrogen Evolution Reaction Catalysts and Their Practical Implementation. *J. Phys. Chem. Lett.* **2015**, *6*, 951−957.

(14) Benck, J. D.; Hellstern, T. R.; Kibsgaard, J.; Chakthranont, P.; Jaramillo, T. F. Catalyzing the Hydrogen Evolution Reaction (HER) with Molybdenum Sulfide Nanomaterials. *ACS Catal.* **2014**, *4*, 3957−3971.

(15) Hou, Y.; Abrams, B. L.; Vesborg, P. C.; Bjorketun, M. E.; Herbst, K.; Bech, L.; Setti, A. M.; Damsgaard, C. D.; Pedersen, T.; Hansen, O.; Rossmeisl, J.; Dahl, S.; Norskov, J. K.; Chorkendorff, I. Bioinspired Molecular Co-catalysts Bonded to a Silicon Photocathode for Solar Hydrogen Evolution. *Nat. Mater.* **2011**, *10*, 434−438.

(16) Ganatra, R.; Zhang, Q. Few-Layer MoS_2: A Promising Layered Semiconductor. *ACS Nano* **2014**, *8*, 4074−4099.

(17) Yan, Y.; Xia, B.; Qi, X.; Wang, H.; Xu, R.; Wang, J. Y.; Zhang, H.; Wang, X. Nano-tungsten Carbide Decorated Graphene as Co-catalysts for Enhanced Hydrogen Evolution on Molybdenum Disulfide. *Chem. Commun.* **2013**, *49*, 4884−4886.

(18) Yan, Y.; Ge, X.; Liu, Z.; Wang, J. Y.; Lee, J. M.; Wang, X. Facile Synthesis of Low Crystalline MoS_2 Nanosheet-Coated CNTs for Enhanced Hydrogen Evolution Reaction. *Nanoscale* **2013**, *5*, 7768−7771.

(19) Bonde, J.; Moses, P. G.; Jaramillo, T. F.; Nørskov, J. K.; Chorkendorff, I. Hydrogen Evolution on Nano-particulate Transition Metal Sulfides. *Faraday Discuss.* **2009**, *140*, 219−231.

(20) Jaramillo, T. F.; Jorgensen, K. P.; Bonde, J.; Nielsen, J. H.; Horch, S.; Chorkendorff, I. b. Identification of Active Edge Sites for Electrochemical H_2 Evolution from MoS_2 Nanocatalysts. *Science* **2007**, *317*, 100−102.

(21) Kong, D.; Wang, H.; Cha, J. J.; Pasta, M.; Koski, K. J.; Yao, J.; Cui, Y. Synthesis of MoS_2 and $MoSe_2$ Films with Vertically Aligned Layers. *Nano Lett.* **2013**, *13*, 1341−1347.

(22) Chung, D. Y.; Park, S. K.; Chung, Y. H.; Yu, S. H.; Lim, D. H.; Jung, N.; Ham, H. C.; Park, H. Y.; Piao, Y.; Yoo, S. J.; Sung, Y. E. Edge-Exposed MoS_2 Nano-assembled Structures as Efficient Electrocatalysts for Hydrogen Evolution Reaction. *Nanoscale* **2014**, *6*, 2131−2136.

(23) Kibsgaard, J.; Chen, Z.; Reinecke, B. N.; Jaramillo, T. F. Engineering the Surface Structure of MoS_2 to Preferentially Expose Active Edge Sites for Electrocatalysis. *Nat. Mater.* **2012**, *11*, 963−969.

DOI: 10.1021/acsami.5b03399
ACS Appl. Mater. Interfaces 2015, 7, 14113−14122

(24) Wang, T.; Gao, D.; Zhuo, J.; Zhu, Z.; Papakonstantinou, P.; Li, Y.; Li, M. Size-Dependent Enhancement of Electrocatalytic Oxygen-Reduction and Hydrogen-Evolution Performance of MoS_2 Particles. *Chem.—Eur. J.* **2013**, *19*, 11939−11948.
(25) Wang, T.; Liu, L.; Zhu, Z.; Papakonstantinou, P.; Hu, J.; Liu, H.; Li, M. Enhanced Electrocatalytic Activity for Hydrogen Evolution Reaction from Self-Assembled Monodispersed Molybdenum Sulfide Nanoparticles on an Au Electrode. *Energy Environ. Sci.* **2013**, *6*, 625−633.
(26) Zhang, L.; Wu, H. B.; Yan, Y.; Wang, X.; Lou, X. W. Hierarchical MoS_2 Microboxes Constructed by Nanosheets with Enhanced Electrochemical Properties for Lithium Storage and Water Splitting. *Energy Environ. Sci.* **2014**, *7*, 3302−3306.
(27) Yang, T.; Chen, Y.; Qu, B.; Mei, L.; Lei, D.; Zhang, H.; Li, Q.; Wang, T. Construction of 3D Flower-Like MoS_2 Spheres with Nanosheets as Anode Materials for High-Performance Lithium Ion Batteries. *Electrochim. Acta* **2014**, *115*, 165−169.
(28) Xie, J.; Zhang, H.; Li, S.; Wang, R.; Sun, X.; Zhou, M.; Zhou, J.; Lou, X. W.; Xie, Y. Defect-Rich MoS_2 Ultrathin Nanosheets with Additional Active Edge Sites for Enhanced Electrocatalytic Hydrogen Evolution. *Adv. Mater.* **2013**, *25*, 5807−5813.
(29) Yan, Y.; Xia, B.; Li, N.; Xu, Z.; Fisher, A.; Wang, X. Vertically Oriented MoS_2 and WS_2 Nanosheets Directly Grown on Carbon Cloth as Efficient and Stable 3-Dimensional Hydrogen-Evolving Cathodes. *J. Mater. Chem. A* **2015**, *3*, 131−135.
(30) Bollinger, M. V.; Lauritsen, J. V.; Jacobsen, K. W.; Nørskov, J. K.; Helveg, S.; Besenbacher, F. One-Dimensional Metallic Edge States in MoS_2. *Phys. Rev. Lett.* **2001**, *87*, 196803.
(31) Gopalakrishnan, D.; Damien, D.; Shaijumon, M. M. MoS_2 Quantum Dot-Interspersed Exfoliated MoS_2 Nanosheets. *ACS Nano* **2014**, *8*, 5297−5303.
(32) Wang, Y.; Ou, J. Z.; Balendhran, S.; Chrimes, A. F.; Mortazavi, M.; Yao, D. D.; Field, M. R.; Latham, K.; Bansal, V.; Friend, J. R.; Zhuiykov, S.; Medhekar, N. V.; Strano, M. S.; Kalantar-Zadeh, K. Electrochemical Control of Photoluminescence in Two-Dimensional MoS_2 Nanoflakes. *ACS Nano* **2013**, *7*, 10083−10093.
(33) Xu, S.; Li, D.; Wu, P. One-Pot, Facile, and Versatile Synthesis of Monolayer MoS_2/WS_2 Quantum Dots as Bioimaging Probes and Efficient Electrocatalysts for Hydrogen Evolution Reaction. *Adv. Funct. Mater.* **2015**, *25*, 1127−1136.
(34) Gopalakrishnan, D.; Damien, D.; Li, B.; Gullappalli, H.; Pillai, V. K.; Ajayan, P. M.; Shaijumon, M. M. Electrochemical Synthesis of Luminescent MoS_2 Quantum Dots. *Chem. Commun.* **2015**, *51*, 6293−6296.
(35) Zhou, F.; Liang, Y.; Liu, W. Ionic Liquid Lubricants: Designed Chemistry for Engineering Applications. *Chem. Soc. Rev.* **2009**, *38*, 2590−2599.
(36) Shang, N. G.; Papakonstantinou, P.; Sharma, S.; Lubarsky, G.; Li, M.; McNeill, D. W.; Quinn, A. J.; Zhou, W.; Blackley, R. Controllable Selective Exfoliation of High-Quality Graphene Nanosheets and Nanodots by Ionic Liquid Assisted Grinding. *Chem. Commun.* **2012**, *48*, 1877−1879.
(37) Benson, J.; Xu, Q.; Wang, P.; Shen, Y.; Sun, L.; Wang, T.; Li, M.; Papakonstantinou, P. Tuning the Catalytic Activity of Graphene Nanosheets for Oxygen Reduction Reaction via Size and Thickness Reduction. *ACS Appl. Mater. Interfaces* **2014**, *6*, 19726−19736.
(38) Fukushima, T.; Kosaka, A.; Ishimura, Y.; Yamamoto, T.; Takigawa, T.; Ishii, N.; Aida, T. Molecular Ordering of Organic Molten Salts Triggered by Single-Walled Carbon Nanotubes. *Science* **2003**, *300*, 2072−2074.
(39) Fukushima, T.; Aida, T. Ionic Liquids for Soft Functional Materials with Carbon Nanotubes. *Chemistry* **2007**, *13*, 5048−5058.
(40) Shakourian-Fard, M.; Jamshidi, Z.; Bayat, A.; Kamath, G. Meta-Hybrid Density Functional Theory Study of Adsorption of Imidazolium- and Ammonium-Based Ionic Liquids on Graphene Sheet. *J. Phys. Chem. C* **2015**, *119*, 7095−7108.
(41) Loh, G. C.; Pandey, R.; Yap, Y. K.; Karna, S. P. MoS_2 Quantum Dot: Effects of Passivation, Additional Layer, and h-BN Substrate on Its Stability and Electronic Properties. *J. Phys. Chem. C* **2015**, *119*, 1565−1574.
(42) Coleman, J. N.; Lotya, M.; O'Neill, A.; Bergin, S. D.; King, P. J.; Khan, U.; Young, K.; Gaucher, A.; De, S.; Smith, R. J.; Shvets, I. V.; Arora, S. K.; Stanton, G.; Kim, H. Y.; Lee, K.; Kim, G. T.; Duesberg, G. S.; Hallam, T.; Boland, J. J.; Wang, J. J.; Donegan, J. F.; Grunlan, J. C.; Moriarty, G.; Shmeliov, A.; Nicholls, R. J.; Perkins, J. M.; Grieveson, E. M.; Theuwissen, K.; McComb, D. W.; Nellist, P. D.; Nicolosi, V. Two-Dimensional Nanosheets Produced by Liquid Exfoliation of Layered Materials. *Science* **2011**, *331*, 568−571.
(43) Splendiani, A.; Sun, L.; Zhang, Y.; Li, T.; Kim, J.; Chim, C. Y.; Galli, G.; Wang, F. Emerging Photoluminescence in Monolayer MoS_2. *Nano Lett.* **2010**, *10*, 1271−1275.
(44) Mak, K. F.; Lee, C.; Hone, J.; Shan, J.; Heinz, T. F. Atomically Thin MoS_2: A New Direct-Gap Semiconductor. *Phys. Rev. Lett.* **2010**, 105.
(45) Eda, G.; Yamaguchi, H.; Voiry, D.; Fujita, T.; Chen, M.; Chhowalla, M. Photoluminescence from Chemically Exfoliated MoS_2. *Nano Lett.* **2011**, *11*, 5111−5116.
(46) Wilcoxon, J.; Samara, G. Strong Quantum-Size Effects in a Layered Semiconductor: MoS_2 Nanoclusters. *Phys. Rev. B* **1995**, *51*, 7299−7302.
(47) Ramakrishna Matte, H. S. S.; Gomathi, A.; Manna, A. K.; Late, D. J.; Datta, R.; Pati, S. K.; Rao, C. N. R. MoS_2 and WS_2 Analogues of Graphene. *Angew. Chem., Int. Ed.* **2010**, *49*, 4059−4062.
(48) Yan, Y.; Xia, B.; Ge, X.; Liu, Z.; Wang, J. Y.; Wang, X. Ultrathin MoS_2 Nanoplates with Rich Active Sites as Highly Efficient Catalyst for Hydrogen Evolution. *ACS Appl. Mater. Interfaces* **2013**, *5*, 12794−12798.
(49) Li, H.; Zhang, Q.; Yap, C. C. R.; Tay, B. K.; Edwin, T. H. T.; Olivier, A.; Baillargeat, D. From Bulk to Monolayer MoS_2: Evolution of Raman Scattering. *Adv. Funct. Mater.* **2012**, *22*, 1385−1390.
(50) Nayak, A. P.; Pandey, T.; Voiry, D.; Liu, J.; Moran, S. T.; Sharma, A.; Tan, C.; Chen, C.; Li, L.; Chhowalla, M.; Lin, J.; Singh, A. K.; Akinwande, D. Pressure-Dependent Optical and Vibrational Properties of Monolayer Molybdenum Disulfide. *Nano Lett.* **2015**, *15*, 346−353.
(51) Zhang, X.; Qiao, X. F.; Shi, W.; Wu, J. B.; Jiang, S.; Tan, P. H. Phonon and Raman Scattering of Two-Dimensional Transition Metal Dichalcogenides from Monolayer, Multilayer to Bulk Material. *Chem. Soc. Rev.* **2015**, *44*, 2757−2785.
(52) Zhang, W.; Chuu, C. P.; Huang, J. K.; Chen, C. H.; Tsai, M. L.; Chang, Y. H.; Liang, C. T.; Chen, Y. Z.; Chueh, Y. L.; He, J. H.; Chou, M. Y.; Li, L. J. Ultrahigh-Gain Photodetectors Based on Atomically Thin Graphene-MoS_2 Heterostructures. *Sci. Rep.* **2014**, *4*, 3826.
(53) Nguyen, E. P.; Carey, B. J.; Daeneke, T.; Ou, J. Z.; Latham, K.; Zhuiykov, S.; Kalantar-zadeh, K. Investigation of Two-Solvent Grinding-Assisted Liquid Phase Exfoliation of Layered MoS_2. *Chem. Mater.* **2015**, *27*, 53−59.
(54) Benck, J. D.; Chen, Z.; Kuritzky, L. Y.; Forman, A. J.; Jaramillo, T. F. Amorphous Molybdenum Sulfide Catalysts for Electrochemical Hydrogen Production: Insights into the Origin of their Catalytic Activity. *ACS Catal.* **2012**, *2*, 1916−1923.
(55) Liu, X.; Zhou, W.; Yang, L.; Li, L.; Zhang, Z.; Ke, Y.; Chen, S. Nitrogen and Sulfur Co-doped Porous Carbon Derived from Human Hair as Highly Efficient Metal-Free Electrocatalysts for Hydrogen Evolution Reactions. *J. Mater. Chem. A* **2015**, *3*, 8840−8846.
(56) Trasatti, S.; Petrii, O. A. Real Surface Area Measurements in Electrochemistry. *J. Electroanal. Chem.* **1992**, *327*, 353−376.
(57) Vilekar, S. A.; Fishtik, I.; Datta, R. Kinetics of the Hydrogen Electrode Reaction. *J. Electrochem. Soc.* **2010**, *157*, B1040.
(58) Conway, B. E.; Tilak, B. V. Interfacial Processes Involving Electrocatalytic Evolution and Oxidation of H_2, and the Role of Chemisorbed H. *Electrochim. Acta* **2002**, *47*, 3571−3594.
(59) Skúlason, E.; Tripkovic, V.; Björketun, M. E.; Gudmundsdóttir, S.; Karlberg, G.; Rossmeisl, J.; Bligaard, T.; Jónsson, H.; Nørskov, J. K. Modeling the Electrochemical Hydrogen Oxidation and Evolution Reactions on the Basis of Density Functional Theory Calculations. *J. Phys. Chem. C* **2010**, *114*, 18182−18197.

DOI: 10.1021/acsami.5b03399
ACS Appl. Mater. Interfaces 2015, 7, 14113−14122

(60) Ji, S.; Yang, Z.; Zhang, C.; Liu, Z.; Tjiu, W. W.; Phang, I. Y.; Zhang, Z.; Pan, J.; Liu, T. Exfoliated MoS_2 Nanosheets As Efficient Catalysts for Electrochemical Hydrogen Evolution. *Electrochim. Acta* **2013**, *109*, 269−275.
(61) Varrla, E.; Backes, C.; Paton, K. R.; Harvey, A.; Gholamvand, Z.; McCauley, J.; Coleman, J. N. Large-Scale Production of Size-Controlled MoS2 Nanosheets by Shear Exfoliation. *Chem. Mater.* **2015**, *27*, 1129−1139.
(62) Seo, B.; Jung, G. Y.; Sa, Y. J.; Jeong, H. Y.; Cheon, J. Y.; Lee, J. H.; Kim, H. Y.; Kim, J. C.; Shin, H. S.; Kwak, S. K.; Joo, S. H. Monolayer-Precision Synthesis of Molybdenum Sulfide Nanoparticles and Their Nanoscale Size Effects in the Hydrogen Evolution Reaction. *ACS Nano* **2015**, *9*, 3728−3739.
(63) Wang, H.; Lu, Z.; Kong, D.; Sun, J.; Hymel, T. M.; Cui, Y. Electrochemical Tuning of MoS_2 Nanoparticles on Three-Dimensional Substrate for Efficient Hydrogen Evolution. *ACS Nano* **2014**, *8*, 4940−4947.
(64) Wu, Z.; Fang, B.; Wang, Z.; Wang, C.; Liu, Z.; Liu, F.; Wang, W.; Alfantazi, A.; Wang, D.; Wilkinson, D. P. MoS_2 Nanosheets: A Designed Structure with High Active Site Density for the Hydrogen Evolution Reaction. *ACS Catal.* **2013**, *3*, 2101−2107.
(65) Sun, X.; Dai, J.; Guo, Y.; Wu, C.; Hu, F.; Zhao, J.; Zeng, X.; Xie, Y. Semimetallic Molybdenum Disulfide Ultrathin Nanosheets as an Efficient Electrocatalyst for Hydrogen Evolution. *Nanoscale* **2014**, *6*, 8359−8367.
(66) Skúlason, E.; Tripkovic, V.; Björketun, M. E.; Gudmundsdóttir, S.; Karlberg, G.; Rossmeisl, J.; Bligaard, T.; Jónsson, H.; Nørskov, J. K. Modeling the Electrochemical Hydrogen Oxidation and Evolution Reactions on the Basis of Density Functional Theory Calculations. *J. Phys. Chem. C* **2010**, *114*, 18182−18197.
(67) Nolan, H.; McEvoy, N.; O'Brien, M.; Berner, N. C.; Yim, C.; Hallam, T.; McDonald, A. R.; Duesberg, G. S. Molybdenum Disulfide/Pyrolytic Carbon Hybrid Electrodes for Scalable Hydrogen Evolution. *Nanoscale* **2014**, *6*, 8185−8191.
(68) Chen, W. F.; Muckerman, J. T.; Fujita, E. Recent Developments in Transition Metal Carbides and Nitrides as Hydrogen Evolution Electrocatalysts. *Chem. Commun.* **2013**, *49*, 8896−8909.
(69) Kibsgaard, J.; Jaramillo, T. F. Molybdenum Phosphosulfide: An Active, Acid-Stable, Earth-Abundant Catalyst for the Hydrogen Evolution Reaction. *Angew. Chem., Int. Ed.* **2014**, *53*, 14433−14437.
(70) Chen, Z.; Cummins, D.; Reinecke, B. N.; Clark, E.; Sunkara, M. K.; Jaramillo, T. F. Core−Shell MoO_3−MoS_2 Nanowires for Hydrogen Evolution: A Functional Design for Electrocatalytic Materials. *Nano Lett.* **2011**, *11*, 4168−4175.
(71) McCrory, C. C.; Jung, S.; Peters, J. C.; Jaramillo, T. F. Benchmarking Heterogeneous Electrocatalysts for the Oxygen Evolution Reaction. *J. Am. Chem. Soc.* **2013**, *135*, 16977−16987.
(72) Li, Y.; Yu, Y.; Huang, Y.; Nielsen, R. A.; Goddard, W. A.; Li, Y.; Cao, L. Engineering the Composition and Crystallinity of Molybdenum Sulfide for High-Performance Electrocatalytic Hydrogen Evolution. *ACS Catal.* **2015**, *5*, 448−455.

DOI: 10.1021/acsami.5b03399
ACS Appl. Mater. Interfaces 2015, 7, 14113−14122